

Evaluation of Oxygen Adsorption Based on the Electric Properties of SnO₂ Semiconductor Gas Sensors

Koichi Suematsu,[†] Kiyomi Yamada,¹ Masayoshi Yuasa,^{††}
Tetsuya Kida,^{†††} and Kengo Shimanoe^{*}

Department of Energy and Material Sciences, Faculty of Engineering Science,
Kyushu University, Kasuga, Fukuoka 816-8580, Japan

¹Department of Molecular and Material Sciences, Interdisciplinary Graduate School of Engineering Sciences,
Kyushu University, Kasuga, Fukuoka 816-8580, Japan

(Received June 6, 2016; accepted August 3, 2016)

Keywords: SnO₂, nanoparticles, oxygen adsorption, equilibrium constant

We successfully prepared SnO₂ nanoparticles of two different sizes by hydrothermal synthesis and calcination at 400 °C to evaluate the oxygen adsorption equilibrium constant $K_{(\text{O}^{2-}_{\text{ad}})}$ on a particle surface. The $K_{(\text{O}^{2-}_{\text{ad}})}$ values were calculated from the relationship between the electric resistance and the oxygen partial pressure (P_{O_2}). The $K_{(\text{O}^{2-}_{\text{ad}})}$ values of 7 and 17 nm SnO₂ nanoparticles were almost in the same range when the donor densities of these nanoparticles are the same. Additionally, the sensor responses of these nanoparticles to hydrogen were affected by the surface-area-to-volume ratio because the $K_{(\text{O}^{2-}_{\text{ad}})}$ values are the same. Thus, we propose that the $K_{(\text{O}^{2-}_{\text{ad}})}$ value can be evaluated on the basis of the relationship between the electric resistance and P_{O_2} .

1. Introduction

Tin dioxide (SnO₂) is the main semiconductor used to detect combustible gases in commercial applications as well as in research on gas sensors. Such resistive-type gas sensors have been utilized as gas leakage detectors and for air pollution monitoring,^(1–3) and can also be used as detectors for breath gases.^(4,5) Combustible gases are typically detected by measuring the change in the electric resistance of SnO₂ particles. In air atmosphere, SnO₂ particles adsorb the dissociative oxygen with negative charge, and an electron depletion region is formed on the particle surface. In contrast, combustible gases consume the adsorbed oxygen via a surface combustion reaction and thus reduce the electron depletion region. In short, oxygen adsorption increases the electric resistance, whereas a surface combustion reaction decreases the electric resistance of SnO₂ particles. A difference in the electric resistance indicates the presence of combustible gases. Therefore, the key to gas detection is the oxygen adsorption amount and species. Thus understanding the oxygen adsorption ability of the SnO₂ surface is very important for gas sensors.

*Corresponding author: e-mail: shimanoe.kengo.695@m.kyushu-u.ac.jp

[†]Present address: Chemical and Texture Research Institute, Fukuoka Industrial Technology Center, Chikushino, Fukuoka 818-8540, Japan

^{††}Present address: Faculty of Humanity-Oriented Science and Engineering, Kinki University, Iizuka, Fukuoka 820-8555, Japan

^{†††}Present address: Department of Applied Chemistry and Biochemistry, Kumamoto University, Kumamoto 860-8555, Japan

Recently, we have proposed the existence of a relationship between the oxygen adsorption and the electric properties, on the basis of the production of an electron depletion layer.^(6,7) According to the proposal, the electric resistance of SnO₂ gas sensors is proportional to the square root of the oxygen partial pressure ($P_{O_2}^{1/2}$), or fourth root of the oxygen partial pressure ($P_{O_2}^{1/4}$), and these relationships determine the oxygen adsorption species as being either O⁻ or O²⁻.⁽⁷⁾ For the evaluation of such a relationship, we have recently proposed that a gas treatment system equipped with a catalytic chamber and an absorbent chamber has to be put on the conventional gas flow system.⁽⁸⁾ The resulting oxygen adsorption species on the SnO₂ surface at 350 °C in extremely dry atmosphere was O²⁻. Under this condition, the oxygen adsorption is expressed by the following reaction, and the electric resistance of SnO₂ gas sensors is explained by the following equation.^(7,8)



$$\frac{R}{R_0} = \left\{ \frac{c^2}{4} + \frac{6N_D}{a} \cdot (K_{(O^{2-}_{ad})} \cdot P_{O_2})^{\frac{1}{2}} \right\}^{\frac{1}{2}} + \frac{c}{2} \quad (2)$$

Here, R/R_0 is the relative resistance, R and R_0 are the electric resistances in the atmosphere with and without oxygen, respectively, N_D is the donor density, a is the crystallite radius, $K_{(O^{2-}_{ad})}$ is the oxygen adsorption equilibrium constant of O²⁻, and c is a constant. The equilibrium constant $K_{(O^{2-}_{ad})}$ is expressed as the ratio of k_1 to k_{-1} ($K_{(O^{2-}_{ad})} = k_1/k_{-1}$); here, k_1 and k_{-1} are the rate constants of the forward and reverse reactions of Eq. (1), respectively. The $K_{(O^{2-}_{ad})}$ value indicates the oxygen adsorption ability on the SnO₂ surface as O²⁻, and determines the intrinsic properties on the sensitivity of SnO₂ gas sensors. However, this value has been difficult to evaluate experimentally. Therefore, in this study, we attempted to evaluate the $K_{(O^{2-}_{ad})}$ value on the basis of the relationship between R/R_0 and $P_{O_2}^{1/4}$ from experimental results using SnO₂ nanoparticles of two different sizes. Basically, the $K_{(O^{2-}_{ad})}$ value should be independent of the SnO₂ crystallite size when the calcination temperature of SnO₂ is the same, because the surface state of the SnO₂ crystals is determined by the calcination process. SnO₂ nanoparticles of different sizes were prepared by hydrothermal synthesis and calcination, which is the same for each SnO₂.⁽⁹⁾ Additionally, we can assume that these donor densities are almost in the same range, because the calcination temperature strongly affects the donor density.⁽¹⁰⁾ Here, donor density is the intrinsic factor of SnO₂ nanoparticles and is not dependent on the oxygen adsorption. The density of electron charge dependent on the oxygen adsorption is defined as the “carrier concentration”. Moreover, we compared the sensor responses to hydrogen using size-controlled SnO₂ nanoparticles, and discussed the responses on the basis of the characteristics of SnO₂ nanoparticles such as a and $K_{(O^{2-}_{ad})}$.

2. Materials and Methods

2.1 Preparation and evaluation of materials

The size-controlled SnO₂ nanoparticles solutions were prepared by hydrothermal synthesis starting from SnCl₄·5H₂O and NH₄HCO₃.^(9,11) For the preparation of small-SnO₂ (S-SnO₂) nanoparticles, an aqueous solution of SnCl₄ (1 mol/L) was added dropwise into the aqueous solution

of NH_4HCO_3 (1 mol/L) and left for half a day to obtain a white precipitate. The thus obtained stannic acid gel was dispersed in deionized water after washing to remove the Cl^- by centrifugation, and the solution pH was adjusted to 10.5 by mixing with an ammonia solution. Subsequently, the S- SnO_2 dispersed solution was prepared by hydrothermal synthesis at 200 °C for 3 h at 10 MPa with stirring at 600 rpm.

Large- SnO_2 (L- SnO_2) nanoparticles were prepared by hydrothermal synthesis via seed-mediated growth using S- SnO_2 nanoparticles as seed particles. The stannic acid gel, as described above, was dispersed in deionized water, and the pH was adjusted to 13.5 by mixing with tetramethylammonium hydroxide (TMAH) to prepare the growth solution. An appropriate amount of S- SnO_2 sol was added to the growth solution, and this mixed solution was hydrothermally treated at 250 °C for 10 h at 10 MPa with stirring at 600 rpm. Detailed conditions for obtaining the size-controlled SnO_2 nanoparticle solutions are described in a previous report.⁽⁹⁾

The size of the nanoparticles in the solutions was determined by dynamic light scattering (DLS) analysis using a DLS spectrophotometer (LPA-3000/3100, Otsuka Electronics). The crystal structure was analyzed by an X-ray diffraction (XRD; RINT 2100, Rigaku) with copper $\text{K}\alpha$ radiation, and the average crystallite size was estimated using Scherrer's equation on the basis of the XRD patterns at (110), (101), and (211) peaks. The obtained nanoparticles were observed using field-emission scanning electron microscopy (FE-SEM; JSM-6340F, JEOL).

2.2 Sensor fabrication and evaluation of electronic resistance

A thin-film-type sensing layer was fabricated by the spin-coating method on an alumina substrate printed with a comb-type Au electrode (90 mm distance between lines, 64 mm² sensing area). The thickness of the sensing layers was controlled to ca. 200 nm. The obtained devices were attached to the gas flow apparatus equipped with an electric furnace, and calcined at 400 °C for 3 h to obtain the sensor device. The measurement system for this study was constructed with various chambers for the gas treatment system, electric resistance measurement (sensor chamber), and oxygen sensor, as described in Fig. 1(a). The gas treatment system is necessary for evaluating the electric resistance accurately.⁽⁸⁾ First, the sample gases of various concentrations of oxygen with nitrogen were passed through the gas treatment system, which is equipped with a catalyst and adsorbent chambers, to eliminate the impurities of the gases. Subsequently, the purified gases were passed through the sensor chamber and oxygen sensor chamber to evaluate the electric resistance of the device and P_{O_2} in the atmosphere, respectively. Oxygen partial pressure was controlled by changing the mixing ratio of oxygen (or synthetic air) to nitrogen gases from commercial gas cylinders, and the total gas flow rate of sample gases was set at 80 cm³/min with mass flow controllers (SEC-series; HORIBA STEC). Here, the electric resistances were evaluated at 350 °C.

Finally, the sensor responses to 200 and 1000 ppm hydrogen at 350 °C for each sensor device were evaluated using a conventional gas flow apparatus equipped with an electric furnace and without using the gas treatment system, as shown in Fig. 1(b). The sample gases of the hydrogen in air were prepared by mixing with synthetic air gas from commercial gas cylinders. The sensor response to hydrogen was defined as R_a/R_g , where R_a is the electric resistance in synthetic air and R_g is that in air containing hydrogen.

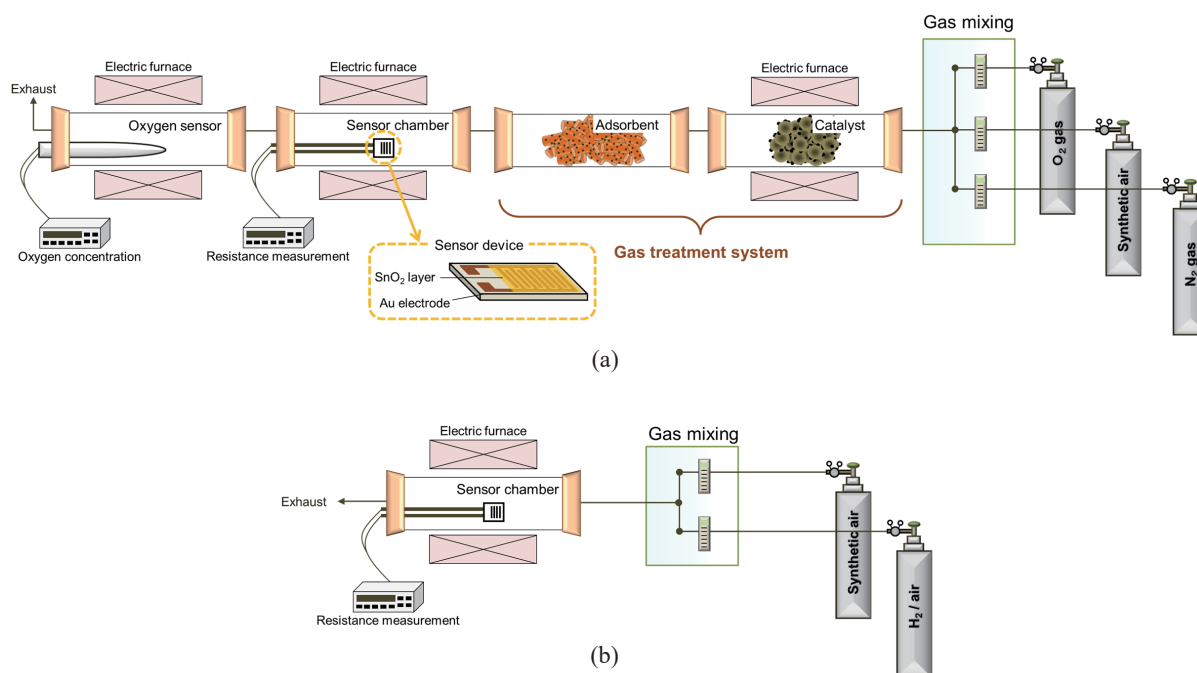


Fig. 1. (Color online) Schematic drawing of the electric resistance measurement apparatuses (a) constructed with the chamber for gas treatment system, electric resistance measurement, and oxygen sensor, and (b) conventional system.

3. Results and Discussion

Figure 2(a) shows the colloidal particle distribution (DLS) of S-SnO₂ and L-SnO₂ nanoparticles; no significant particle aggregation appeared in each nanoparticle. The particle distribution range is clearly different for each nanoparticle. The average colloidal particle sizes of the S-SnO₂ and L-SnO₂ nanoparticles were 5 and 17 nm, respectively. The XRD patterns of the dried and calcined powders using S-SnO₂ and L-SnO₂ are shown in Fig. 2(b); powder drying and calcining were carried out under the conditions of 120 °C for 12 h and 400 °C for 3 h, respectively. These XRD patterns correspond well to the cassiterite-type SnO₂ structure (JCPDS 41-1445), and the SnO₂ was successfully crystallized during the hydrothermal treatment at 200 °C because SnO₂ peaks clearly appeared on the XRD pattern of the dried SnO₂ powders. The estimated crystallite sizes of the dried nanoparticles of S-SnO₂ and L-SnO₂ were 4 and 17 nm, respectively. These sizes are consistent with the average colloidal particle sizes from the DLS measurement. Thus, S-SnO₂ and L-SnO₂ nanoparticles are highly dispersed in each solution. In addition, the estimated crystallite sizes of calcined nanoparticles for S-SnO₂ and L-SnO₂ were 7 and 17 nm, respectively. Figure 2(c) shows the SEM images of S-SnO₂ and L-SnO₂ nanoparticles calcined at 400 °C, and no apparent aggregation of the nanoparticles are observed in both sizes of SnO₂. Accordingly, we obtained SnO₂ nanoparticles of two different sizes under the same calcination conditions, which indicates that the donor densities of both SnO₂ nanoparticles are almost in the same range.

The electric resistance at various oxygen partial pressures [$P_{O_2} = 0 (=N_2)$, 0.01, 0.05, 0.1, 0.4, 1 atm] was measured at 350 °C using S-SnO₂ and L-SnO₂ thin-film sensors. The relative resistance is

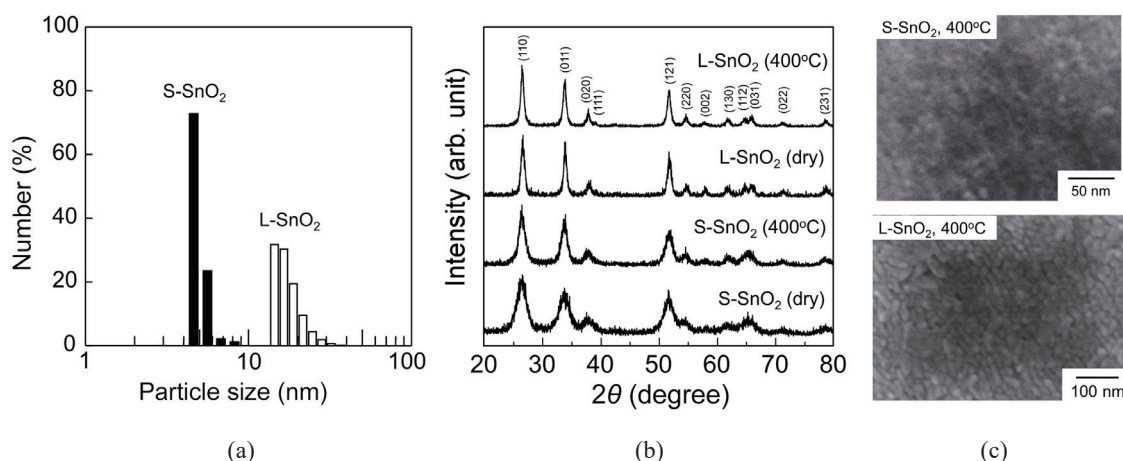


Fig. 2. (a) Particle size distribution, (b) XRD patterns, and (c) SEM images of both S-SnO₂ and L-SnO₂ nanoparticles.

determined on the basis of the ratio of the electric resistance in the atmosphere, including oxygen, to that in nitrogen (R/R_{N_2}). The relationships of the relative resistance to both $P_{O_2}^{1/2}$ and $P_{O_2}^{1/4}$ are shown in Figs. 3(a) and 3(b), respectively. Clearly, the relative resistance shows a nonlinear relationship with $P_{O_2}^{1/2}$, while it shows a linear relationship with $P_{O_2}^{1/4}$ in the operated P_{O_2} range regardless of the particle size. Thus, the oxygen is adsorbed as O^{2-} on the particle surface; in addition, the amount of O^- adsorption on the particle surface is negligibly small, as described in a previous report.⁽⁷⁾ The $K_{(O^{2-}_{ad})}$ value was calculated from the theoretical equation Eq. (2) using the slopes of the approximated straight lines in Fig. 3(b). The obtained slope and estimated $K_{(O^{2-}_{ad})}$ values of S-SnO₂ and L-SnO₂ nanoparticles are compiled in Table 1. Here, N_D is assumed as $5.0 \times 10^{18} \text{ cm}^{-3}$ ($5.0 \times 10^{-3} \text{ nm}^{-3}$). Accordingly, these $K_{(O^{2-}_{ad})}$ values are almost in the same range. The $K_{(O^{2-}_{ad})}$ value of S-SnO₂ nanoparticles was 3.2 times as large as that of L-SnO₂ nanoparticles. However, the reason for such a small difference is as yet unclear. Nevertheless, the obtained $K_{(O^{2-}_{ad})}$ values indicate that the oxygen adsorption abilities of both SnO₂ surfaces are the same, and are independent of the crystallite size. On the other hand, the relative resistance is significantly affected by crystallite size throughout the entire measured P_{O_2} range. The estimated surface-area-to-volume ratios of S-SnO₂ (7 nm) and L-SnO₂ (17 nm) are shown in Table 1, and the ratio of S-SnO₂ is significantly larger than that of L-SnO₂. Thus, the crystallite size affects the ratio of surface-area-to-volume, and causes the difference in the relative resistance. Therefore, the obtained results correspond well to the theoretical equation Eq. (2) and the $K_{(O^{2-}_{ad})}$ values successfully obtained from the experimental result.

Finally, we evaluated the sensor responses to 200 and 1000 ppm hydrogen using S-SnO₂ and L-SnO₂ thin-film sensors at 350 °C, as shown in Fig. 4. The sensor response of S-SnO₂ nanoparticles is significantly higher than that of L-SnO₂ nanoparticles, regardless of the hydrogen concentration, even though the $K_{(O^{2-}_{ad})}$ values are in the same range. Such difference in the sensor response is caused by the difference in crystallite size, which indicates a difference in the surface-area-to-volume ratio as shown in Table 1. The sensor response using S-SnO₂ is about 3 times larger than that using L-SnO₂, and the ratio of surface-area-to-volume of S-SnO₂ is about 2.5 times

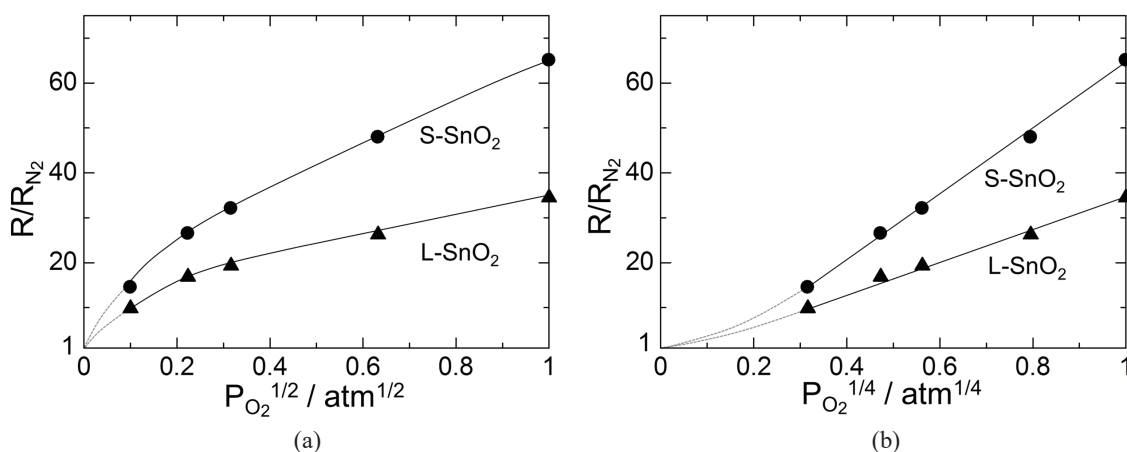


Fig. 3. Relative resistances of S-SnO₂ and L-SnO₂ nanoparticles as functions of (a) $P_{O_2}^{1/2}$ and (b) $P_{O_2}^{1/4}$ at 350 °C.

Table 1

Slopes of approximate line in Fig. 3(b), $K_{(O^{2-})}$ values at 350 °C and surface-area-to-volume ratio of S-SnO₂ and L-SnO₂ nanoparticles.

Sample	Slope/atm ^{-1/4}	$K_{(O^{2-})}/nm^4 \cdot atm$	Surface-area-to-volume ratio/nm ⁻¹
S-SnO ₂	73	3.8×10^{11}	0.86
L-SnO ₂	35	1.2×10^{11}	0.35

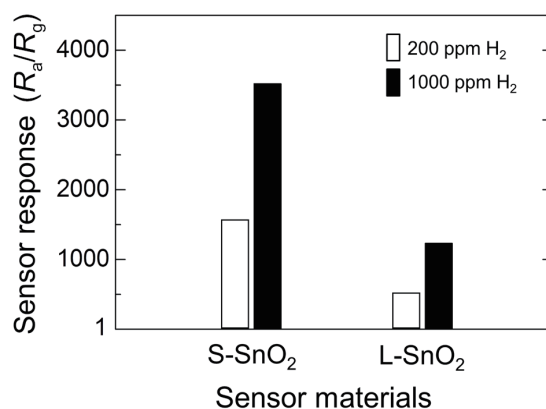


Fig. 4. Sensor responses to 200 and 1000 ppm hydrogen at 350 °C using S-SnO₂ and L-SnO₂ nanoparticles.

larger than that of L-SnO₂. Thus, the enhancement of the sensor response to hydrogen is caused by increasing the surface-area-to-volume ratio when the donor density and oxygen adsorption equilibrium are the same, and it fundamentally agrees with a previously reported theory of the gas sensing mechanism.⁽⁷⁾

4. Conclusions

To calculate the oxygen adsorption equilibrium constant $K_{(O^{2-}_{ad})}$ on the basis of the evaluation of electric properties, we measured the electric resistance at various oxygen partial pressures using highly pure gases passed through a gas treatment system. SnO₂ nanoparticles of two sizes, namely 7 and 17 nm, were prepared by hydrothermal synthesis and calcination. Thin-film-type sensing layers were fabricated by the spin-coating method, and the sensor devices were obtained by sintering at 400 °C. The relative resistance (R/R_{N_2}) of both sensors had a linear relationship with $P_{O_2}^{1/4}$ at 350 °C in extremely dry atmosphere, which indicates that oxygen is adsorbed as O²⁻ on the particle surface. Moreover, according to the slope of the approximate straight line between R/R_{N_2} and $P_{O_2}^{1/4}$, the $K_{(O^{2-}_{ad})}$ values of both sensors were almost in the same range. This indicates that the $K_{(O^{2-}_{ad})}$ value is independent of the crystallite size of SnO₂. On the other hand, the sensor responses to hydrogen of small SnO₂ nanoparticles were clearly higher than those of large SnO₂ nanoparticles even though these $K_{(O^{2-}_{ad})}$ values were almost the same. This is because the surface-area-to-volume ratio of SnO₂ crystals significantly affected the sensor response. According to our results, the $K_{(O^{2-}_{ad})}$ value, which is important surface information of the gas sensors, can be evaluated easily from the relationship between the electric resistance and the P_{O_2} . Moreover, the sensor response to hydrogen is strongly affected by the crystallite size because the phenomenon of the surface area is susceptible to the whole particle region. Therefore, these results confirm a material design to enhance the sensor response; for example, increasing the oxygen adsorption equilibrium boosts the sensor response of the semiconductor gas sensors. In the future, it is necessary to investigate the effect of the surface modification such as elemental doping on the oxygen adsorption equilibrium, to understand the importance of the surface modification for semiconductor gas sensors.

Acknowledgements

This work was partly supported by a Grant-in-Aid for Scientific Research (B) 16H04219 from the Ministry of Education, Science, Sport and Culture of Japan.

References

- 1 Figaro Engineering Inc.: Homepage of Figaro Engineering Inc., <http://www.figaro.co.jp/> (accessed April 2016).
- 2 FIS Inc.: Homepage of FIS Inc., <http://www.fisinc.co.jp/> (accessed April 2016).
- 3 New Cosmos Electric Co., Ltd.: Homepage of New Cosmos Electric Co., Ltd.: <https://www.new-cosmos.co.jp/> (accessed April 2016).
- 4 K. Suematsu, Y. Shin, N. Ma, T. Oyama, M. Sasaki, M. Yuasa, T. Kida, and K. Shimanoe: *Anal. Chem.* **87** (2015) 8407.
- 5 K. I. Choi, H. J. Kim, Y. C. Kang, and J.-H. Lee: *Sens. Actuators, B* **194** (2014) 371.
- 6 N. Yamazoe and K. Shimanoe: *J. Electrochem. Soc.* **155** (2008) J93.
- 7 N. Yamazoe, K. Suematsu, and K. Shimanoe: *Sens. Actuators, B* **163** (2012) 128.
- 8 K. Suematsu, M. Yuasa, T. Kida, N. Yamazoe, and K. Shimanoe: *J. Electrochem. Soc.* **161** (2014) B123.
- 9 T. Kida, S. Fujiyama, K. Suematsu, M. Yuasa, and K. Shimanoe: *J. Phys. Chem. C* **117** (2013) 17574.
- 10 J. Maier and W. Göpel: *J. Solid State Chem.* **72** (1998) 293.
- 11 N. S. Baik, G. Sakai, N. Miura, and N. Yamazoe: *J. Am. Ceram. Soc.* **83** (2000) 2983.